


## Green Synthesized Iron Oxide Nanoparticles from Rice Husk for Ciprofloxacin and Ibuprofen Adsorption

Habib I. Adamu <sup>1</sup>; Muhammad D. Faruruwa<sup>2</sup>; Modupe M. Adeyemi<sup>2</sup>; and Wasiu B. Tomori<sup>2</sup>

<sup>1</sup>Department of Chemistry, Nigerian Defence Academy Kaduna, Nigeria/Department of Environmental Management, Kaduna State University Kaduna, Nigeria. <sup>2</sup>Department of Chemistry, Nigerian Defence Academy Kaduna, Nigeria/Federal University of Technology Akure, Nigeria.

Corresponding author: [habibadamu99@kasu.edu.ng](mailto:habibadamu99@kasu.edu.ng)

DOI: <https://doi.org/10.62154/ajastr.2025.018.010673>

### Abstract

Pharmaceutical contamination of water, particularly by ciprofloxacin and ibuprofen, poses serious environmental and health risks. This study investigates the use of rice husk-derived iron oxide nanoparticles (Fe<sub>3</sub>O<sub>4</sub> NPs) for their removal, utilizing a green synthesis approach that repurposes rice husk, an abundant agricultural byproduct, to produce cost-effective and eco-friendly adsorbents. Comprehensive characterization using techniques such as FTIR, UV-Vis, DLS, SEM, EDS, XRD, and BET confirmed the successful synthesis and desirable properties of the nanoparticles. Batch adsorption experiments revealed high removal efficiencies, with optimal conditions determined for adsorbent dose, shaking time, initial concentration, pH, and temperature. Maximum removal efficiencies were 98.92% for ciprofloxacin and 96.60% for ibuprofen under optimized conditions: pH 7, shaking times of 15 and 25 minutes, adsorbent dose of 100 mg, initial ciprofloxacin and ibuprofen concentrations of 10 mg/L and 4 mg/L, and temperatures of 320K and 300K, respectively. Thermodynamic analysis showed that ciprofloxacin adsorption was spontaneous (negative  $\Delta G$ ), exothermic, and became more favorable at higher temperatures, whereas ibuprofen adsorption was non-spontaneous, endothermic, and decreased with temperature. Kinetic studies indicated that adsorption followed pseudo-second-order kinetics, with equilibrium data best fitting the Langmuir model for ciprofloxacin and the Freundlich model for ibuprofen. Maximum adsorption capacities were 4.87 mg/g for ciprofloxacin and 12.49 mg/g for ibuprofen. Reusability tests showed a slight decline in efficiency over four cycles (4.30% for ciprofloxacin, 25.83% for ibuprofen), demonstrating the nanoparticles' potential as a sustainable and cost-effective solution for pharmaceutical wastewater treatment.

**Keywords:** Rice Husk, Green Synthesis, Nanoparticles, Ciprofloxacin, Ibuprofen, Adsorption.

### Introduction

Water contamination by pharmaceuticals is an escalating environmental issue, with antibiotics like ciprofloxacin and non-steroidal anti-inflammatory drugs (NSAIDs) such as ibuprofen frequently detected in various water bodies (Gomes, 2024). These contaminants enter aquatic environments through multiple pathways, including human and veterinary use, improper disposal, and agricultural runoff. Their persistence and bioactivity pose

significant risks to aquatic life and human health, necessitating effective removal strategies (Singh *et al.*, 2024). Traditional water treatment methods often fall short in effectively removing these pharmaceuticals, highlighting the need for innovative and efficient solutions.

Nanotechnology has emerged as a promising approach for environmental remediation, with iron oxide nanoparticles ( $\text{Fe}_3\text{O}_4$  NPs) gaining significant attention due to their high surface area, magnetic separability, and adsorption capacity (Shakorflow *et al.*, 2023). Although numerous studies have explored the use of iron nanoparticles for water treatment, the majority rely on chemical synthesis methods that are expensive and environmentally detrimental (Mansoori *et al.*, 2021). Green synthesis, utilizing plant extracts or agricultural byproducts, offers a sustainable and cost-effective alternative. This study hypothesizes that iron oxide nanoparticles synthesized via a green method using rice husk extract will effectively adsorb ciprofloxacin and ibuprofen from aqueous solutions, providing an efficient and eco-friendly solution for pharmaceutical wastewater treatment. While several studies have examined iron nanoparticles prepared from rice husk, this research offers distinct advantages. Unlike previous works that primarily focus on structural characterization or heavy metal removal, this study investigates the adsorption efficiency and mechanisms for pharmaceutical contaminants, a relatively underexplored area. Additionally, the unique composition of rice husk-derived  $\text{Fe}_3\text{O}_4$  NPs is hypothesized to enhance adsorption through synergistic interactions between the bioactive surface functionalities and the pharmaceutical molecules (Moradi *et al.*, 2016).

To bridge this research gap, this study aims to synthesize iron oxide nanoparticles ( $\text{Fe}_3\text{O}_4$  NPs) using rice husk extract as a green, sustainable alternative to chemically synthesized nanoparticles and to characterize the synthesized nanoparticles to confirm their structural, morphological, and adsorption properties. It further seeks to evaluate the adsorption efficiency of  $\text{Fe}_3\text{O}_4$  NPs in removing ciprofloxacin and ibuprofen under varying experimental conditions, including pH, adsorbent dose, contact time, temperature, and initial concentration. Additionally, the study analyzes the adsorption kinetics, isotherms, and thermodynamics to understand the mechanisms governing the removal process while also assessing the reusability of the nanoparticles to determine their potential for long-term and sustainable wastewater treatment applications.

By leveraging the multifunctional properties of rice husk-derived  $\text{Fe}_3\text{O}_4$  NPs, this study not only provides a sustainable solution for pharmaceutical removal but also promotes the valorization of agricultural waste. The findings contribute to advancing green nanotechnology applications in water treatment, offering a scalable and eco-friendly approach to mitigating pharmaceutical contamination.

## **Methodology**

### **Preparation of rice husk extract**

To harness the potential of agro waste, specifically rice husk, the local rice mill provided the raw material which was meticulously processed. The rice husk underwent a thorough

cleansing with tap water followed by a drying phase in the shade. Subsequently, the dried husk was finely pulverized utilizing an electric blender (Silver Crest). For the experimental procedure, 10g of the finely ground rice husk was precisely weighed using an analytical balance (Adventurer Ohaus AR310MS-H-S Wincon). The measured quantity was then carefully transferred into a 250 mL Erlenmeyer flask. The extraction process commenced with the addition of 100 mL of distilled water at a controlled temperature of 40°C. The extraction operation ran smoothly for 2 hours under constant stirring at 500rpm/min using a magnetic stirrer (MS-H-S Wincon), ensuring efficient mixing and extraction of the desired components (Faisal *et al.*, 2021).

#### **Iron oxide nanoparticle synthesis using rice husk extract**

The synthesis process of iron oxide ( $\text{Fe}_3\text{O}_4$ ) nanoparticles revolved around reducing  $\text{Fe}^{3+}$  and  $\text{Fe}^{2+}$  ions with rice husk extract acting as both the reducing and stabilizing agent. To initiate the synthesis, a 1.0M solution of  $\text{FeCl}_3$  and a 0.5M solution of  $\text{FeCl}_2$  were prepared from  $\text{FeCl}_3 \cdot 6\text{H}_2\text{O}$  and  $\text{FeCl}_2 \cdot \text{H}_2\text{O}$ . Subsequently, 100 ml of rice husk extract was carefully measured using a measuring cylinder and then transferred into an Erlenmeyer flask.

The experimental setup involved placing the flask on a magnetic stirrer, followed by the gradual addition of a 50 mL solution containing  $\text{Fe}^{3+}$  and  $\text{Fe}^{2+}$  salts in a 2:1 molar ratio. Throughout the reaction progression, the pH of the solution was adjusted by the incremental introduction of a 1M NaOH solution to achieve a pH of 11. The homogenization of the solution continued for 1 hour under constant stirring with the magnetic stirrer to ensure the completion of the reaction. Subsequently, the mixture was subjected to centrifugation at 5000rpm/min for 10 minutes to facilitate the recovery and separation of the nanoparticles. The isolated nanoparticles were treated with five washes of deionized water followed by a final wash with ethanol to eliminate impurities. Following this purification step, the nanoparticles were dried in an oven at 130°C and stored in an airtight container for future use. The successful formation of nanoparticles was indicated by the observable color change in the solution and further validated through UV-visible spectroscopy. This synthesis methodology draws reference from previous works (Mohamed Khalith *et al.*, 2022; Adamu *et al.*, 2023; Faruruwa *et al.*, 2024).

#### **Characterization of the synthesized iron oxide nanoparticles**

For comprehensive analysis of the synthesized nanoparticles, a range of characterization techniques were employed. The Fourier-transform infrared spectroscopy (FT-IR) analysis was conducted utilizing the Shimadzu FTIR 8400S instrument. Spectra data were acquired in transmittance mode across the 4000-400  $\text{cm}^{-1}$  range to elucidate the chemical composition and functional groups present. The Rigaku Mini flex 6g X-ray diffraction system was utilized with monochromatic Cu K $\alpha$  radiation with data collection spanned the  $2\theta$  range of 20 to 70, providing insights into the structural properties of the synthesized materials. The surface morphology was examined through scanning electron microscopy using the JOEL JSM 7600F instrument equipped with Energy Dispersive X-ray (EDX)

capabilities, enabling detailed visualization and elemental analysis. The optical characteristics of the nanoparticles, the T70 PG Instruments' UV-Spectrophotometer was employed, shedding light on their unique optical properties and behavior. The size and size distribution of the nanoparticles was scrutinized using the Malvern Panalytical Zetasizer Range Multi Angle Light Scattering Nano ZS90, offering valuable data on particle size distribution and homogeneity. The thermal stability of the nanoparticles was studied with thermogravimetric analyzer (TGA Q50). The  $pH_{pzc}$  was studied using a procedure described by (Bakatula *et al.*, 2018).

### Batch adsorption of ciprofloxacin and ibuprofen

The adsorption behavior of ciprofloxacin and ibuprofen was investigated through batch adsorption experiments, following the methodology outlined by Ahmadpour *et al.* (2019) and Faruruwa *et al.* (2024). The optimal adsorbent dose was ascertained by varying the adsorbent quantity within the range of 20-100mg. pH levels were adjusted to 3, 5.7, 9, and 11 using 0.1M solutions of HCl and NaOH to explore the impact of acidity and alkalinity on adsorption efficiency. Furthermore, the adsorbate dosage was varied from 2-10 mg/L over a duration of 5-40 minutes and the effect of temperature at 300, 305, 310, 315 and 320K maintaining a consistent shaking speed of 200 rpm throughout the experiments. The specific amount of ciprofloxacin adsorbed under different experimental conditions was calculated using the following equation:

$$q_e = \frac{(C_0 - C_e)V}{W} \quad (1)$$

and

$$\% \text{ Removal} = \frac{C_0 - C_e}{C_0} * 100 \quad (2)$$

where  $q_e$  is the adsorption amount of ciprofloxacin (mg/g) in the solid at equilibrium;  $C_0$  and  $C_e$  are the initial and equilibrium concentrations of pharmaceutical (mg/L), respectively;  $V$  is the volume (mL) of the aqueous solution and  $W$  is the mass (g) of adsorbent used in the experiments.

### Thermodynamic study

The thermodynamic study was conducted at a temperature range of 27° C - 42° C (300-320K) varying the temperatures at 5° C intervals.

The three essential parameters of the thermodynamic study which are the Gibbs free energy ( $\Delta G^\circ$ ), enthalpy change ( $\Delta H^\circ$ ) and entropy change ( $\Delta S^\circ$ ) were evaluated using the Van't Hoff equation. The Gibbs free energy ( $\Delta G^\circ$ ) is expressed as;

$$\Delta G = -RT \ln K_o \quad (3)$$

And

$$K_o = q_e / C_e \quad (4)$$

Where  $R$ ,  $T$  and  $K_o$  are universal gas constant (8.314 J/Kmol), absolute temperature (K) and thermodynamic constant (dimensionless) respectively.

The third principle in thermodynamic expressed the relationship between  $\Delta G^\circ$ ,  $\Delta H^\circ$  and  $\Delta S^\circ$  in the equation

$$\Delta G^\circ = \Delta H^\circ - T\Delta S^\circ \quad (5)$$

Where the  $\Delta G^\circ$ ,  $\Delta H^\circ$  and  $\Delta S^\circ$  are the Gibbs free energy ( $\text{J mol}^{-1}$ ), enthalpy change ( $\text{J mol}^{-1}$ ) and entropy change ( $\text{J mol}^{-1} \text{K}^{-1}$ ). Combining equations 3.3 and 3.5 generate the Van't Hoff equation expressed in equation 3.6.

$$\ln K_o = -\frac{-\Delta H^\circ}{RT} + \frac{\Delta S^\circ}{R} \quad (6)$$

Hence,  $\Delta G^\circ$ ,  $\Delta H^\circ$  and  $\Delta S^\circ$  can be determined from the slope and intercept of the plot of  $\ln K_o$  on the y axis and  $1/T$  on the x axis generate a straight-line with the slope and intercept as  $-\Delta H^\circ/R$  and  $\Delta S^\circ/R$  respectively.

### Kinetic studies

At the optimum conditions studied, adsorption kinetics data was fitted into pseudo first order, pseudo second order and interparticle diffusion and Elovich kinetics models in order to determine its order and mechanism of adsorption. The applicability of the models will be measured by the regression values (Oputu *et al.*, 2022).

The pseudo first order kinetic model was studied according to the integrated rate law equation expressed as:

$$\ln(q_e - q_t) = \ln q_e - k_1 t \quad (7)$$

The Pseudo second order kinetic model integrated rate law equation:

$$\frac{t}{q_t} = \frac{1}{K_2 q_e^2} + \frac{1}{q_e} \quad (8)$$

where  $q_e$  and  $q_t$  (both in  $\text{mg/g}$ ) are the amount of pharmaceutical adsorbed per unit mass of adsorbent at equilibrium and time "t" respectively. The adsorption rate constant ( $k_1$ ) for pharmaceutical sorption will be calculated from the slope of the linear plot  $\ln(q_e - q_t)$  vs time (t) and  $K_2$  is the pseudo- second order rate constant for sorption determined from the plot of  $t/q_e$  vs t (Lunge *et al.*, 2014).

The interparticle diffusion kinetic model equation is given by:

$$qt = k_p t^{1/2} + C \quad (9)$$

where  $qt$  is the amount of adsorbate per unit mass of adsorbent at time t ( $\text{mg/g}$ ),  $K_p$  is the interparticle diffusion rate constant ( $\text{mg/g min}^{1/2}$ ), t is the time (min), and C which indicates the boundary layer effect is the intercept ( $\text{mg/g}$ ) (Ayawei *et al.*, 2017). The data was plotted as  $qt$  versus  $t^{1/2}$ , which gives a straight line according to the interparticle diffusion kinetic model equation.

The Elovich kinetic model equation is given by:

$$qt = \frac{1}{\beta} \ln(\alpha\beta) + \frac{1}{\beta} \ln t \quad (10)$$

where  $qt$  is the amount of adsorbate per unit mass of adsorbent at time t ( $\text{mg/g}$ ),  $\alpha$  is the initial adsorption rate ( $\text{mg/g min}$ ),  $\beta$  is the desorption constant ( $\text{g/mg}$ ), and t is the time (min). The data was plotted as  $qt$  versus  $\ln t$ , which gives a straight line according to the Elovich kinetic model equation. The values of  $\alpha$  and  $\beta$  can be calculated from the intercept

and the slope, respectively. The coefficient of determination ( $R^2$ ) can be used to measure the quality of the fit.

### Adsorption isotherm

To delve into the adsorption mechanism and quantify key adsorption parameters, three isotherm models, namely Langmuir and Freundlich, will be employed to interpret the experimental data effectively.

The equation of the Langmuir isotherm, which suggests a monolayer adsorption onto a surface (Oputu *et al.*, 2022), is given below.

$$qe = q_{max} \frac{K_L C_e}{1 + K_L C_e} \quad (11)$$

The Langmuir's isotherm was transformed into its linear form, as represented in Eq. (12), to determine the adsorption parameters.

$$\frac{1}{q_e} = \frac{1}{K_L q_{max}} \cdot \frac{1}{C_e} + \frac{1}{q_{max}} \quad (12)$$

where  $K_L$  is the Langmuir constant (L/mg) and  $q_{max}$  is the maximum amount of the pharmaceutical adsorbed per gram of adsorbent at equilibrium (mg/g) and  $C_e$  is concentration of adsorbate at equilibrium (mg g<sup>-1</sup>).

A plot of  $1/q_e$  against  $1/C_e$  produces a straight line whose slope and intercept are used to determine values of Langmuir constants  $q_{max}$  and  $K_L$ .

The essential characteristic of the Langmuir isotherm can also be expressed by a dimensionless constant called the separation factor  $R_L$  (Ayawei *et al.*, 2017). Also, it is used to predict the adsorption efficiency of the process, the dimensionless quantity ( $R_L$ ) can be calculated using the following equation:

$$R_L = \frac{1}{1 + K_L C_o} \quad (13)$$

Where  $K_L$  is Langmuir constant (mg/l) and  $C_o$  is initial concentration of adsorbate (mg/l)

$R_L$  values indicate the adsorption to be unfavorable when  $R_L > 1$ , linear when  $R_L < 1$ , favorable when  $0 < R_L < 1$  and irreversible when  $R_L = 0$ .

The equation of the Freundlich isotherm, which suggests that the adsorption occurs onto a heterogeneous surface (Lunge *et al.*, 2014) is as follows.

$$\log q_e = \log k_f + \frac{1}{n} \log C_e \quad (14)$$

where  $K_F$  and  $n$  are the isotherm constants that indicate the capacity and intensity of the adsorption, and  $1/n$  is a function of the strength of adsorption (Oputu *et al.*, 2022). The plot of  $\log(q_e)$  against  $\log(C_e)$  produces a line with intercept value of  $K_F$  and the slope of  $1/n$ .

A value of  $1/n > 1$  suggests weak adsorption while  $1/n < 1$  suggests strong adsorption bond as a result of strong intermolecular attraction within the adsorbent layers. When the value of  $n$  ranges from 2 and 10, indicates good adsorption when the value of  $n$  is between 1- 2, it indicates moderate adsorption capacity and less than one indicating undesirable adsorption capacity (Hamdaoui and Naffrechoux, 2007).

Temkin isotherm model which takes into account the effect of indirect adsorbate/adsorbate interaction on the adsorption process is also assumed that the heat of

adsorption ( $DH_{ads}$ ) of all molecules in the layer decreases linearly as a result of increase surface coverage (Piccin *et al.*, 2011).

The linear form of Temkin isotherm model is given by the following:

$$q_e = \frac{RT}{b} \ln KT + \frac{RT}{b} \ln C_e \quad (15)$$

where  $KT$  is the equilibrium binding constant ( $L \text{ mol}^{-1}$ ) corresponding to the maximum binding energy,  $b$  is related to the adsorption heat,  $R$  is the universal gas constant ( $8.314 \text{ J K}^{-1} \text{ mol}^{-1}$ ) and  $T$  is the temperature (K). Plotting  $q_e$  versus  $\ln(C_e)$  produces a straight line of slope  $RT/b$  and intercept  $(RT \ln KT)/b$  (Piccin *et al.*, 2011).

## Result and Discussion

### FTIR analysis of rice husk extract

The FTIR analysis of rice husk extract, presented in Figure 1, identified key functional groups involved in nanoparticle synthesis and stabilization. A broad peak at  $3272.6 \text{ cm}^{-1}$  corresponds to O–H stretching vibrations, indicating the presence of hydroxyl groups, which play a critical role in reducing iron ions and stabilizing nanoparticles (Mahdavi *et al.*, 2013). The peak at  $2929.7 \text{ cm}^{-1}$  is attributed to C–H stretching, suggesting the presence of organic compounds that may act as capping agents to prevent nanoparticle aggregation (Javed *et al.*, 2020).

A strong absorption band at  $1640.0 \text{ cm}^{-1}$  corresponds to C=C stretching in aromatic rings or C=O stretching in conjugated ketones, aldehydes, or carboxylic acids, indicating the involvement of these groups in stabilizing the synthesized nanoparticles (Yadav *et al.*, 2024). The peak at  $1420.1 \text{ cm}^{-1}$  corresponds to  $\text{CH}_2$  bending vibrations, likely from cellulose or other organic components acting as protective capping agents (Javed *et al.*, 2020). Additionally, peaks at  $1341.8 \text{ cm}^{-1}$  and  $1244.9 \text{ cm}^{-1}$  are associated with C–N stretching of amines or P=O stretching in phosphodiesteres, both of which contribute to nanoparticle reduction and stabilization.

Further, the peaks at  $1151.7 \text{ cm}^{-1}$  and  $1080.9 \text{ cm}^{-1}$  correspond to C–O–C asymmetric stretching, suggesting the presence of polysaccharides such as cellulose and hemicellulose, which enhance nanoparticle stability. A peak at  $998.9 \text{ cm}^{-1}$  is indicative of Si–O–Si asymmetric stretching, confirming the presence of silica, which, although not directly involved in iron oxide nanoparticle synthesis, may influence the process if acting as a structural support (Vikram *et al.*, 2016).

The FTIR analysis confirms that rice husk extract contains diverse functional groups, including hydroxyl, carboxyl, amine, and polysaccharide-based compounds, which facilitate the reduction and stabilization of iron oxide nanoparticles. These bioactive components contribute to the eco-friendly synthesis process and enhance nanoparticle stability.

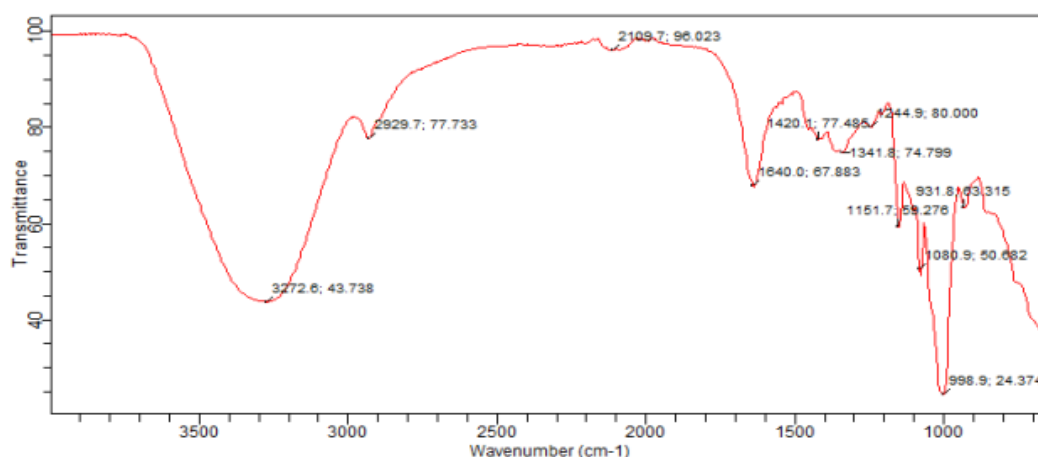


Fig 1.: FTIR spectra of rice husk extract.

## Characterization of the synthesized iron oxide nanoparticles

### UV-Vis analysis

The UV-Vis analysis of the synthesized iron oxide nanoparticles ( $\text{Fe}_3\text{O}_4$  NPs) revealed a strong absorbance peak at 221 nm, characteristic of surface plasmon resonance (SPR) (Vikram *et al.*, 2016). This peak confirms the formation of  $\text{Fe}_3\text{O}_4$  NPs and indicates that the nanoparticles are well-dispersed with minimal aggregation.

The position and intensity of the SPR peak provide insights into the nanoparticles' size and optical properties. Typically, smaller nanoparticles exhibit absorption at lower wavelengths, while larger particles shift toward higher wavelengths (Behzadi *et al.*, 2015). The sharp peak observed at 221 nm suggests that the synthesized nanoparticles are relatively small and uniform in size. A well-defined peak also indicates that the nanoparticles maintain a stable dispersion without significant clustering, which is essential for adsorption applications (Vikram *et al.*, 2016).

The UV-Vis analysis confirms the successful synthesis of  $\text{Fe}_3\text{O}_4$  nanoparticles with a characteristic SPR peak at 221 nm, indicating small, well-dispersed particles with minimal aggregation. These properties enhance their suitability for adsorption-based applications.

### Dynamic light scattering analysis

The Dynamic Light Scattering (DLS) analysis of the synthesized  $\text{Fe}_3\text{O}_4$  nanoparticles revealed a Z-average particle size of 54.24 nm and a polydispersity index (PDI) of 0.476. The Z-average represents the intensity-weighted mean hydrodynamic diameter, indicating that the nanoparticles are within the nanoscale range and suitable for adsorption applications (Yeap *et al.*, 2018).

The PDI value of 0.476 suggests a moderate size distribution, meaning the nanoparticles exhibit some variation in size but remain within an acceptable range for adsorption efficiency. PDI values below 0.05 indicate highly monodisperse systems, while values



between 0.08 and 0.7 suggest moderate dispersion, ensuring consistency in nanoparticle properties (Farkas & Kramar, 2021).

While DLS provides valuable insights into nanoparticle size and distribution, factors such as sample concentration, particle morphology, and potential aggregation can influence the accuracy of measurements (Ahmadpour *et al.*, 2019). The results confirm that the synthesized  $\text{Fe}_3\text{O}_4$  nanoparticles have a relatively uniform size with moderate dispersion, making them suitable for further adsorption studies.

DLS analysis confirmed that the synthesized  $\text{Fe}_3\text{O}_4$  nanoparticles have an average size of 54.24 nm with a moderate size distribution (PDI = 0.476), ensuring suitability for adsorption applications. The findings highlight their stability and uniformity, which are crucial for effective performance in water treatment.

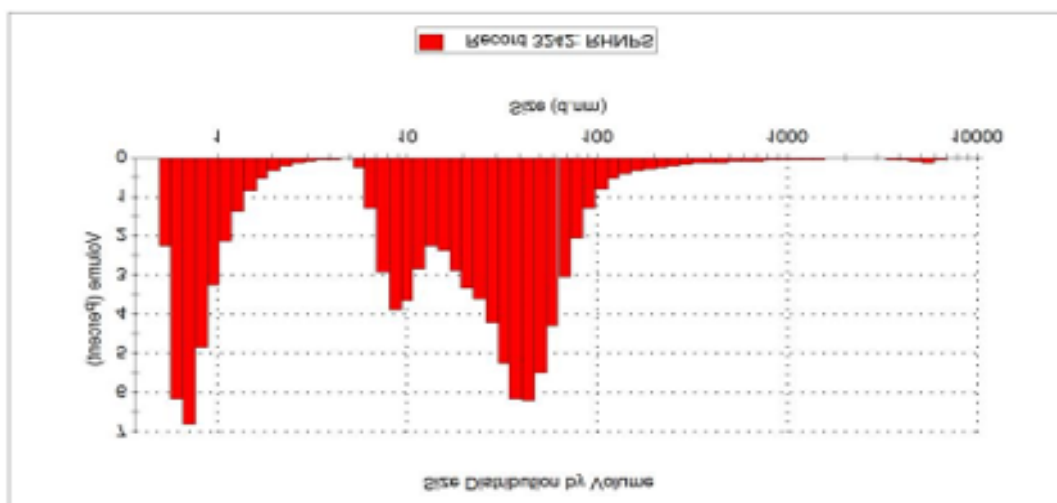


Fig. 2: Size distribution of RHNP against volume

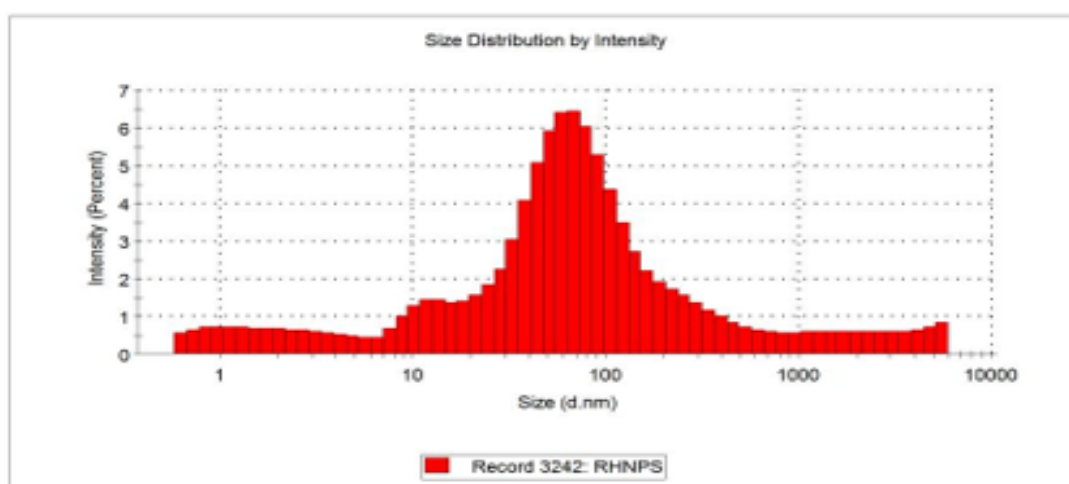


Fig. 3: Size distribution of RHNP against intensity

### FTIR Spectrum analysis of the nanoparticles

The FTIR spectrum of the iron oxide nanoparticles synthesized from rice husk extract (RHNPs) is presented on Fig. 4. Key observations from the analysis include peaks indicative of functional groups such as carboxylic acid at  $3227.87\text{ cm}^{-1}$  and phenol at  $1341.84\text{ cm}^{-1}$ . Notably, the shift of the phenol band from  $3272.60\text{ cm}^{-1}$  in the original rice husk extract FTIR result to  $1341.84\text{ cm}^{-1}$  in the RHNPs spectrum is noteworthy, alongside the persistence of the band for phenol at  $1341.84\text{ cm}^{-1}$ . Additionally, the presence of a band at  $1103.29\text{ cm}^{-1}$  corresponding to amine signifies a shift from the  $1244.90\text{ cm}^{-1}$  observed in the rice husk extract FTIR. These alterations are attributed to the involvement of these compounds in the reduction of iron to form the iron oxide nanoparticles (Zambri *et al.*, 2019). The FTIR spectrum confirmed the successful incorporation of functional groups from rice husk extract, with shifts in key peaks indicating their role in reducing and stabilizing iron oxide nanoparticles.

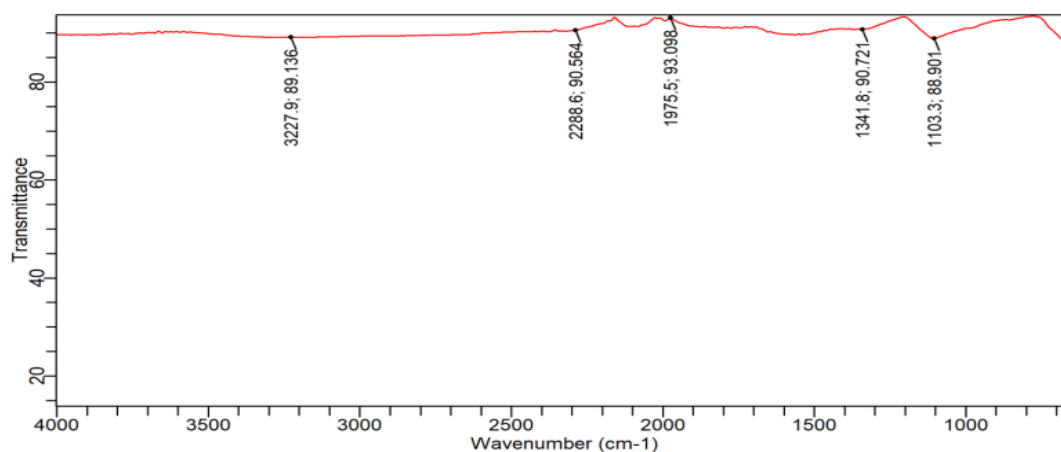
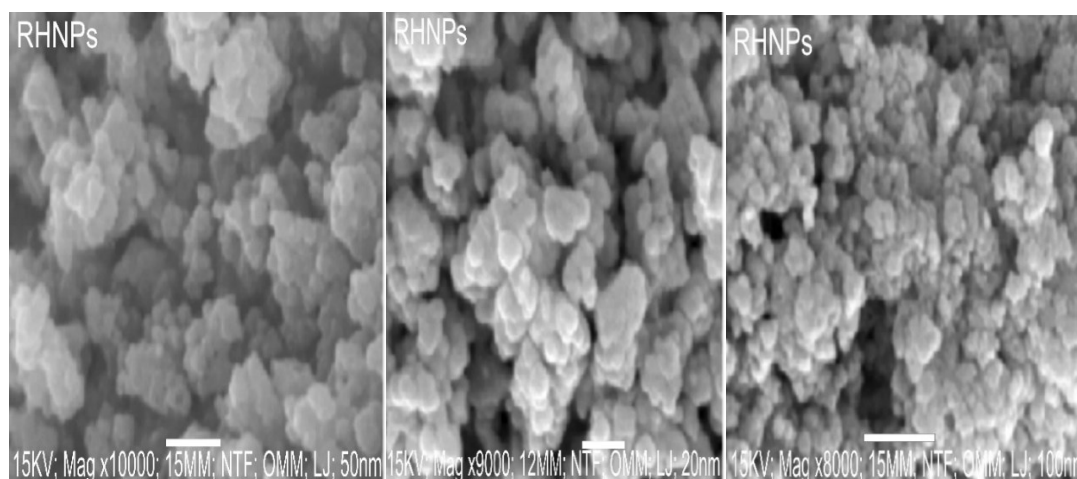


Fig. 4: FTIR spectra of iron oxide nanoparticles synthesized using rice husk extract

### Scanning Electron microscopy and Energy dispersive spectroscopy analysis

The SEM analysis of the synthesized  $\text{Fe}_3\text{O}_4$  nanoparticles revealed irregularly shaped particles with rough edges and visible agglomeration (Plate 1). The particle sizes ranged from 11.90 to 29.23 nm, with an average size of 23.63 nm, which is smaller than the 54.24 nm Z-average obtained from DLS analysis. The variation in size suggests that while the nanoparticles exhibit some degree of polydispersity, they remain within the nanoscale range and suitable for adsorption applications. The observed agglomeration is likely due to magnetic interactions between the nanoparticles, a common characteristic of  $\text{Fe}_3\text{O}_4$ -based materials (Fahmy *et al.*, 2018; Priya *et al.*, 2021).



**Plate 1:** SEM micrograph of RHNPs at magnifications of 10000, 9000 and 8000

The EDS analysis further confirmed the elemental composition of the nanoparticles, with iron (Fe) at 60.96% and oxygen (O) at 25.67%, verifying the successful formation of  $\text{Fe}_3\text{O}_4$ . A minor carbon (C) peak at 18.34% was also detected, which may originate from organic residues in the rice husk extract used during synthesis. The strong Fe and O signals align with the expected stoichiometry of magnetite nanoparticles, supporting the successful synthesis of  $\text{Fe}_3\text{O}_4$  (Zambri *et al.*, 2019).

SEM analysis confirmed that the  $\text{Fe}_3\text{O}_4$  nanoparticles are irregularly shaped with an average size of 23.63 nm, exhibiting some agglomeration due to magnetic interactions. EDS analysis verified the dominant presence of Fe and O, confirming the successful formation of iron oxide nanoparticles.

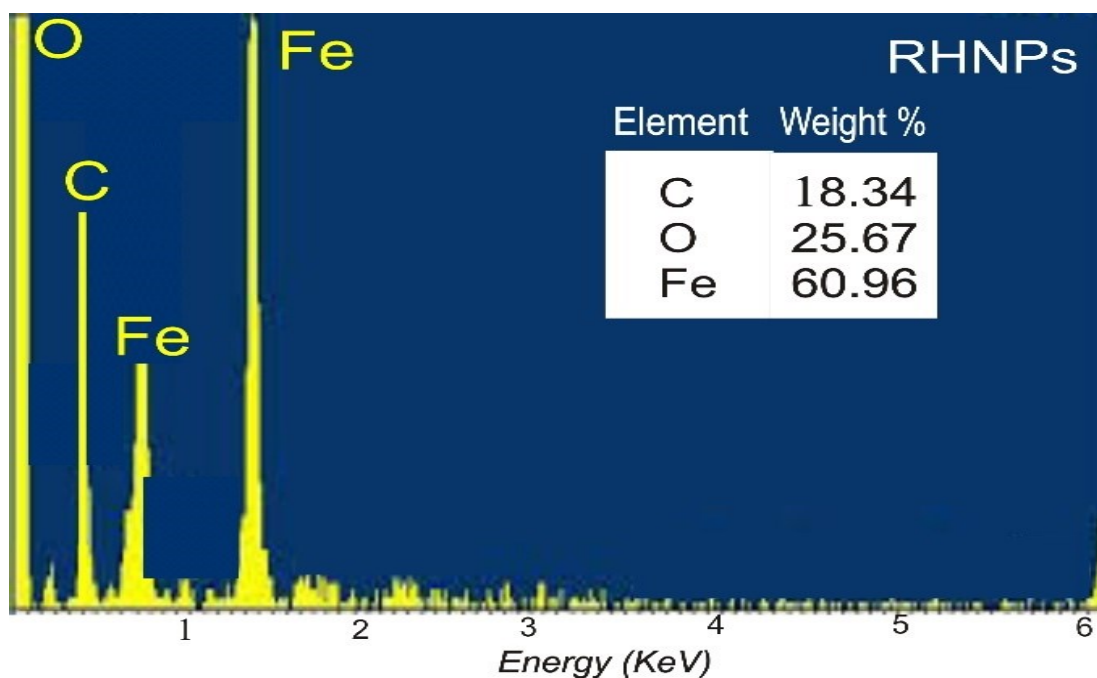


**Fig. 5** Result of the EDS analysis of RHNPs

### X-Ray Diffraction (XRD) analysis

The nanoparticles derived from rice husk extract (depicted in Fig. 6) displayed distinct peaks at  $2\theta$  values of 30.46, 35.86, 37.50, 43.56, 47.68, 54.02, and 57.58 degrees, corresponding to crystallographic planes with Miller index (HKL) values of 022, 112, 222, 004, 133, 224, and 339. Among these, the peak at 35.86 degrees stood out as the most intense, registering a 100% crystal count of magnetite ( $\text{Fe}_3\text{O}_4$ ) with a cubic centered structure. The X-ray diffraction (XRD) pattern closely matched the ICSD collection code: 158505, referencing code: 98-010-9588, and indicated a space group of FD-3M. The crystal size for these nanoparticles was calculated at 60.59 nm using the Debye Scherrer equation. This calculated crystal size slightly exceeded the Z-average of 54.24 nm from the DLS analysis but was notably smaller than the size derived from SEM images using ImageJ software. Despite slight variations in crystal size calculations, all values fell within the nanoscale range, affirming the successful synthesis of iron oxide nanoparticles.

XRD analysis identified characteristic peaks corresponding to  $\text{Fe}_3\text{O}_4$  nanoparticles with a cubic crystal structure. The calculated crystallite size (60.59 nm) was consistent with the nanoscale range, confirming the successful synthesis of iron oxide nanoparticles.

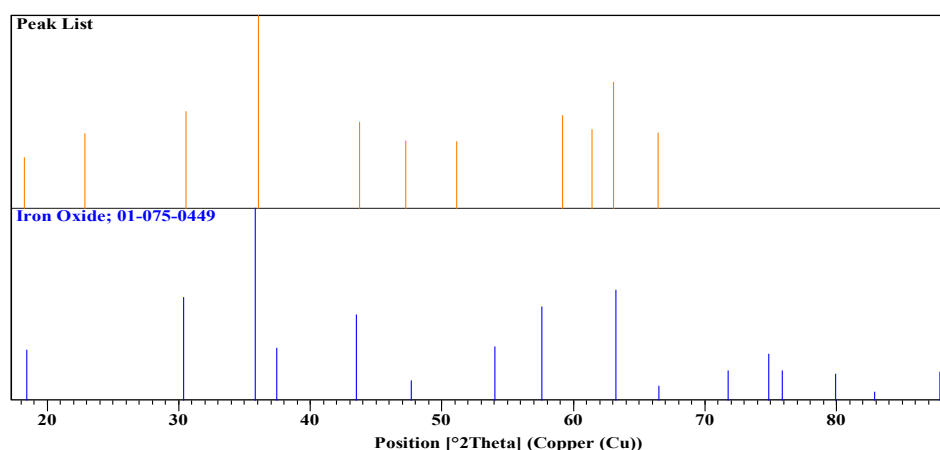


Fig. 6: XRD diffractogram of RHNPs

### The BET analysis

The BET analysis of the nanoparticles showed a Surface Area of  $842.67 \text{ m}^2/\text{g}$  which signifies an exceptionally high surface area, indicating abundant interaction sites for various reactions. This characteristic is advantageous for applications like catalysis, leveraging the increased active sites for enhanced performance. In contrast, the Langmuir Surface Area of  $47.25 \text{ m}^2/\text{g}$  notably lags behind the BET surface area. This discrepancy implies that the Langmuir model, based on monolayer adsorption, might not comprehensively elucidate the adsorption dynamics on these nanoparticles (Rahman *et al.*, 2021; Kumar Mohanta *et al.*, 2021).

The nanoparticles exhibited a high BET surface area ( $842.67 \text{ m}^2/\text{g}$ ), indicating abundant active sites for adsorption. The mesoporous nature, confirmed by the isotherm plot, enhances their suitability for contaminant removal.

The substantial Pore Volume of  $0.60356 \text{ cm}^3/\text{g}$ , coupled with the extensive BET surface area, suggests a porous structure within the nanoparticles. This structural attribute holds promise for applications requiring both high surface area and porosity, such as drug delivery systems or adsorption processes (Kaasalainen *et al.*, 2017). The adherence to a Type II Adsorption Isotherm (Fig. 7) reflects a wide pore size distribution in the material, indicative of multilayer adsorption behavior at elevated pressures. This trend aligns with mesoporous materials characterized by pore diameters ranging from 2 to 50 nm. The observed Hysteresis Condensation Range spanning from 0.05 to 0.78 signals the presence of hysteresis in the adsorption-desorption isotherm, typically associated with capillary condensation in mesopores. The broad relative pressure range hints at a diverse mesopore size distribution within the nanoparticles (Toncon-Leal *et al.*, 2021; Nsubuga *et al.*, 2023). The BET analysis underscores the highly porous nature of the iron oxide nanoparticles derived from rice husk extract, showcasing a favorable combination of substantial surface area and porosity. The Type II isotherm and hysteresis phenomena further validate the mesoporous characteristics of the nanoparticles, rendering them particularly valuable in catalysis, environmental remediation, and medicinal applications where enhanced surface area and porosity are pivotal for optimal performance.

The nanoparticles exhibited a high BET surface area ( $842.67 \text{ m}^2/\text{g}$ ), indicating abundant active sites for adsorption. The mesoporous nature, confirmed by the isotherm plot, enhances their suitability for contaminant removal.

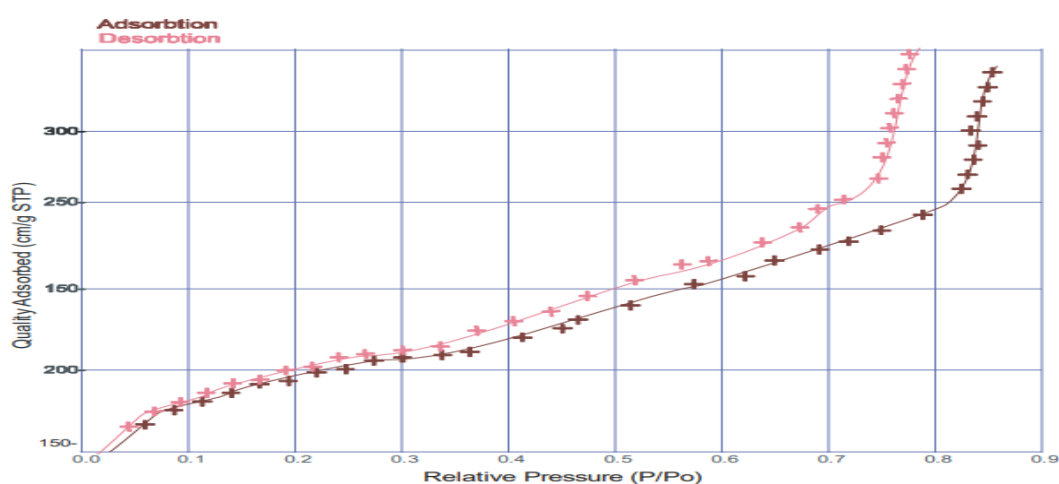


Fig 7: Isotherm linear plot of RHNP

### Result of Batch Adsorption Studies for the Adsorption of Ciprofloxacin and Ibuprofen Effect of shaking time and adsorbent dose on the adsorption of ciprofloxacin and ibuprofen

The adsorption efficiency of  $\text{Fe}_3\text{O}_4$  nanoparticles for ciprofloxacin and ibuprofen increased with higher adsorbent doses and longer shaking times, reaching an equilibrium point beyond which no significant improvement was observed (Figures 8 and 9). Increasing the adsorbent dose from 20 mg to 100 mg provided more available surface area and active sites, enhancing adsorption capacity. However, after reaching an optimal dose, further increases led to only marginal improvements, likely due to the saturation of active sites (Nsubuga *et al.*, 2023).

For ciprofloxacin, the highest removal efficiency (86.08%) was achieved at 100 mg adsorbent dose and 15 minutes shaking time. Beyond this, adsorption slightly declined, suggesting equilibrium had been reached. Similarly, for ibuprofen, adsorption peaked at 96.60% under the same adsorbent dose but at a longer shaking time of 25 minutes. The extended time for ibuprofen may be due to its molecular interactions differing from those of ciprofloxacin (Al-Musawi *et al.*, 2021).

These findings align with previous studies showing that increasing adsorbent quantity enhances removal efficiency up to a saturation point (Bachheti *et al.*, 2019; Ha *et al.*, 2021). The improved adsorption efficiency is attributed to higher surface area, stronger concentration gradients, and enhanced chemical interactions between  $\text{Fe}_3\text{O}_4$  nanoparticles and pharmaceutical molecules (Nithya *et al.*, 2023).

Adsorption efficiency increased with adsorbent dose and shaking time, reaching equilibrium at 15 minutes for ciprofloxacin (86.08%) and 25 minutes for ibuprofen (96.60%). Further increases in adsorbent dose had minimal impact, indicating surface site saturation. These results confirm the strong adsorption potential of  $\text{Fe}_3\text{O}_4$  nanoparticles for pharmaceutical contaminants

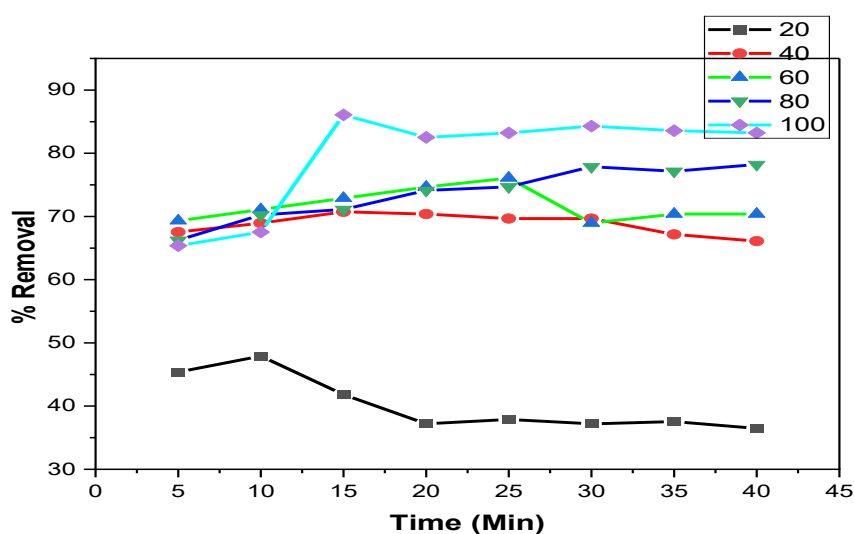
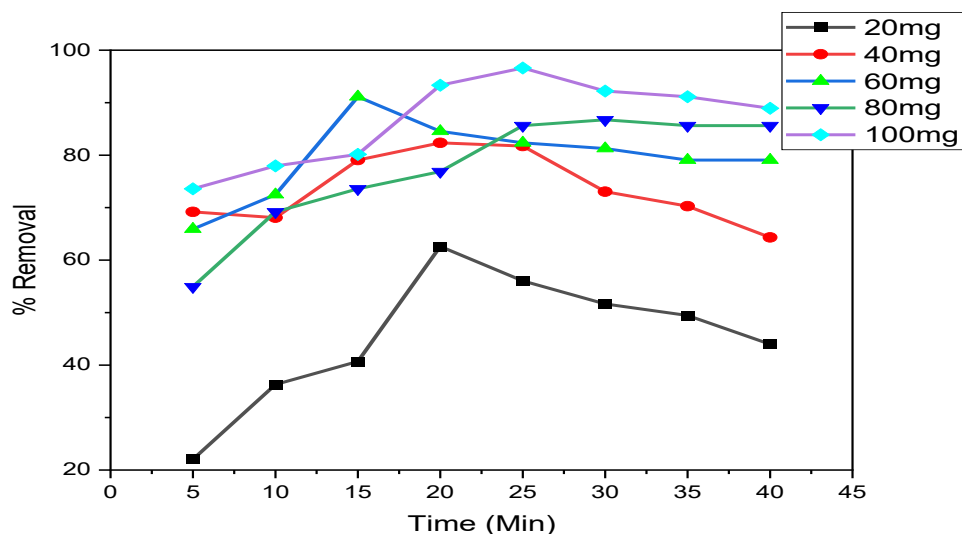


Fig. 8: Effect of Adsorbent Dose and Contact Time on Ciprofloxacin Adsorption Efficiency



**Fig. 9:** Effect of Adsorbent Dose and Contact Time on Ibuprofen Adsorption Efficiency

#### Effect of initial adsorbate concentration

The adsorption capacity of  $\text{Fe}_3\text{O}_4$  nanoparticles was influenced by the initial concentration of ciprofloxacin and ibuprofen, with varying trends observed for each contaminant (Figure 10). For ciprofloxacin, adsorption efficiency increased as the initial concentration rose, reaching a maximum removal of 84.51% at 10 mg/L. This trend is attributed to the higher concentration gradient between the solution and the adsorbent, which enhances mass transfer and promotes stronger interactions at the available active sites (Balarak *et al.*, 2021).

In contrast, ibuprofen adsorption did not follow a clear trend, with efficiency fluctuating across different concentrations. This behavior suggests that factors beyond concentration, such as molecular interactions, solubility, and competitive binding, may influence adsorption performance. Similar observations were reported by Nguyen *et al.* (2019), where ibuprofen removal using metal-organic frameworks showed minimal impact from increasing initial concentration.

Ciprofloxacin adsorption improved with increasing concentration, peaking at 84.51% removal at 10 ppm, while ibuprofen adsorption remained inconsistent, indicating a more complex interaction with  $\text{Fe}_3\text{O}_4$  nanoparticles. These findings suggest that adsorbate properties significantly influence adsorption efficiency beyond initial concentration alone.

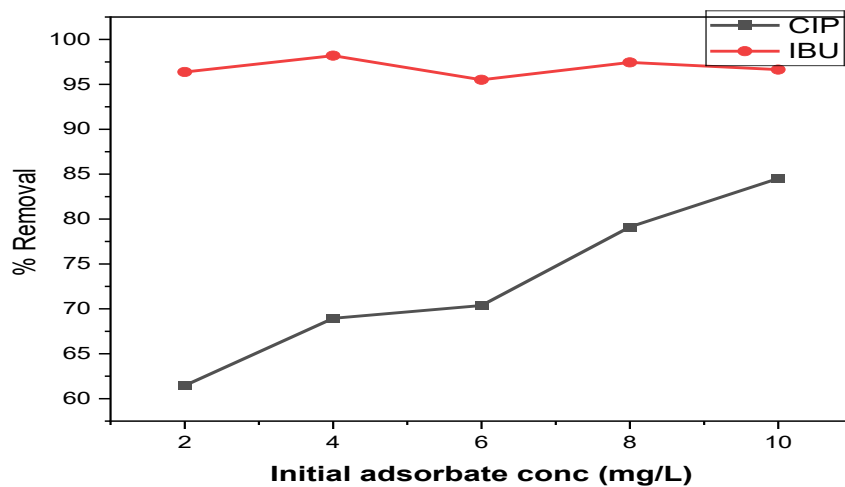


**Fig. 10:** Effect of Initial Ciprofloxacin (CIP) and Ibuprofen (IBU) Concentration on Adsorption Efficiency

#### Effect of pH on the ciprofloxacin and ibuprofen Adsorption

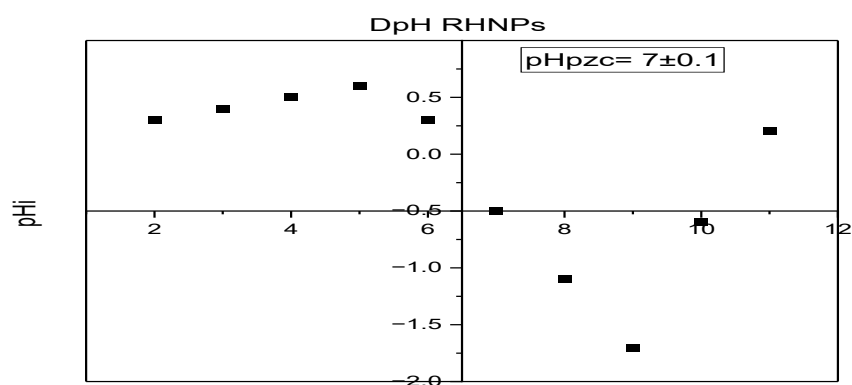


**Fig. 11:** Result of pH<sub>pzc</sub> analysis of RHNP



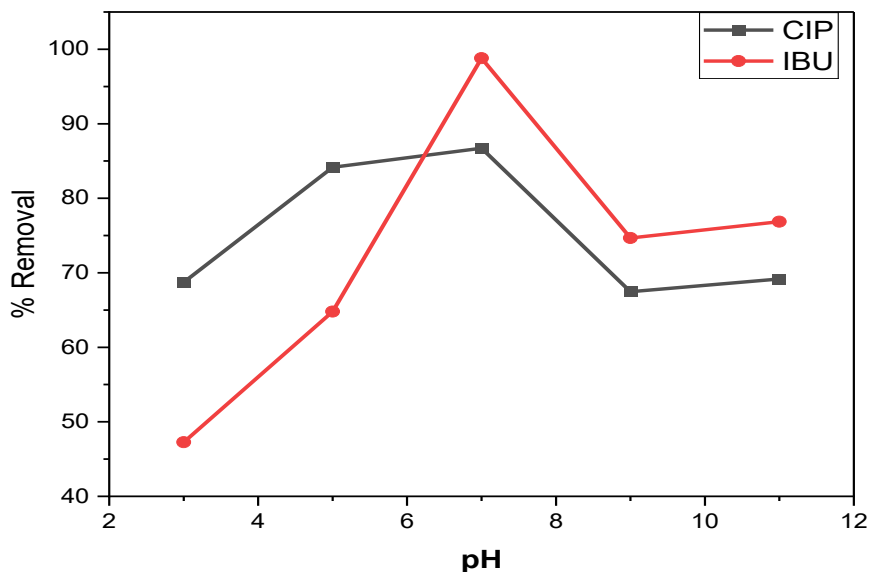


**Fig. 12:** Effect of pH on the Ciprofloxacin and Ibuprofen Adsorption Efficiency

The adsorption efficiency of  $\text{Fe}_3\text{O}_4$  nanoparticles was significantly influenced by pH, which affects both the surface charge of the adsorbent and the ionization state of the pharmaceuticals (Figure 12). The pH<sub>pzc</sub> (point of zero charge) of the nanoparticles was determined to be neutral (pH  $\approx$  6.9) (Figure 11), meaning the surface is positively charged at lower pH values and negatively charged at higher pH values.

For ciprofloxacin, adsorption was highest at pH 7 (94.57%), with efficiency decreasing at both lower and higher pH levels. Ciprofloxacin exists in different ionic forms depending on pH—positively charged at pH < 6.1, neutral between pH 6.1–8.7, and negatively charged at pH > 8.7 (National Center for Biotechnology Information, 2023). The strong adsorption at pH 7 suggests electrostatic attraction between the neutral form of ciprofloxacin and the  $\text{Fe}_3\text{O}_4$  surface, while repulsion at extreme pH values reduces adsorption (Adegoke *et al.*, 2023).

For ibuprofen, maximum adsorption (98% removal) occurred at pH 7, with a decline at both acidic and alkaline conditions. As an organic acid with a pK<sub>a</sub> of 5.2, ibuprofen exists in its neutral form at pH < 5.2 and as an anion at pH > 5.2 (Balarak *et al.*, 2021). Adsorption was most favorable near the pH<sub>pzc</sub>, where electrostatic interactions are minimized, allowing hydrophobic interactions to dominate (Nguyen *et al.*, 2019).

Ciprofloxacin adsorption was highest at pH 7, where neutral molecules interacted most effectively with the  $\text{Fe}_3\text{O}_4$  surface. Ibuprofen also showed peak adsorption at pH 7, but its efficiency declined at higher pH due to electrostatic repulsion. These findings highlight the crucial role of pH in optimizing pharmaceutical removal efficiency using  $\text{Fe}_3\text{O}_4$  nanoparticles.

### Effect of temperature on the adsorption of ciprofloxacin and ibuprofen

Temperature had a significant impact on the adsorption efficiency of  $\text{Fe}_3\text{O}_4$  nanoparticles, but the trends varied for ciprofloxacin and ibuprofen (Figure 13). For ciprofloxacin, adsorption efficiency increased with temperature, reaching a maximum removal of 98.92% between 300–320 K, indicating an endothermic process. The enhanced adsorption at higher temperatures suggests stronger molecular interactions and increased diffusion rates, which facilitate adsorption onto the nanoparticle surface (Xing *et al.*, 2015).

In contrast, ibuprofen adsorption decreased with rising temperature, dropping from 96.60% to 58.22% within the same temperature range. This decline suggests an exothermic process, where higher temperatures reduce adsorption efficiency by weakening adsorbate-adsorbent interactions or increasing ibuprofen solubility, preventing its binding to  $\text{Fe}_3\text{O}_4$  nanoparticles (Garau *et al.*, 2019). Similar behavior has been reported for other organic pollutants, where adsorption is more favorable at lower temperatures (Badawi *et al.*, 2021). Ciprofloxacin adsorption increased with temperature, confirming an endothermic process, while ibuprofen adsorption declined, indicating an exothermic process. These results highlight that temperature influences adsorption differently based on the pharmaceutical's molecular properties and interaction with  $\text{Fe}_3\text{O}_4$  nanoparticles.

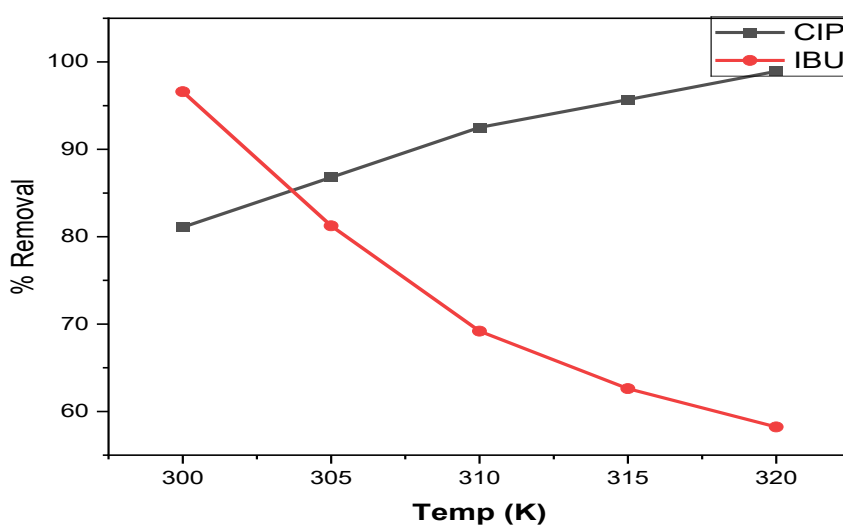


**Fig. 13:** Effect of Temperature on the Ciprofloxacin and Ibuprofen Adsorption Efficiency

### Thermodynamics for the adsorption of CIP and IBU

The thermodynamic parameters for ciprofloxacin and ibuprofen adsorption were evaluated using the Van't Hoff equation, with results summarized in Table 1 and plotted in Figure 14. The negative Gibbs free energy ( $\Delta G$ ) values for ciprofloxacin confirm that adsorption was spontaneous and thermodynamically favorable, with spontaneity increasing as temperature rose. The positive enthalpy change ( $\Delta H$ ) indicates an endothermic process,

meaning higher temperatures enhance adsorption by promoting stronger interactions between ciprofloxacin and  $\text{Fe}_3\text{O}_4$  nanoparticles (Balarak *et al.*, 2021). The positive entropy change ( $\Delta S$ ) suggests increased randomness at the solid-liquid interface, likely due to structural rearrangements upon adsorption (Adegoke *et al.*, 2023).

In contrast, ibuprofen adsorption exhibited positive  $\Delta G$  values, indicating a non-spontaneous process under the tested conditions. The increasing  $\Delta G$  with temperature further suggests that adsorption becomes less favorable at higher temperatures. The negative  $\Delta H$  value confirms an exothermic process, where rising temperatures weaken adsorbate-adsorbent interactions, reducing adsorption efficiency (Nguyen *et al.*, 2019). The positive  $\Delta S$  value implies some degree of disorder at the interface, although the overall process remains thermodynamically unfavorable at higher temperatures (Badawi *et al.*, 2021).

Ciprofloxacin adsorption was spontaneous, endothermic, and became more favorable at higher temperatures, while ibuprofen adsorption was non-spontaneous, exothermic, and declined with increasing temperature. These findings emphasize the distinct thermodynamic behaviors of both pharmaceuticals and the need to optimize temperature conditions for effective adsorption using  $\text{Fe}_3\text{O}_4$  nanoparticles.

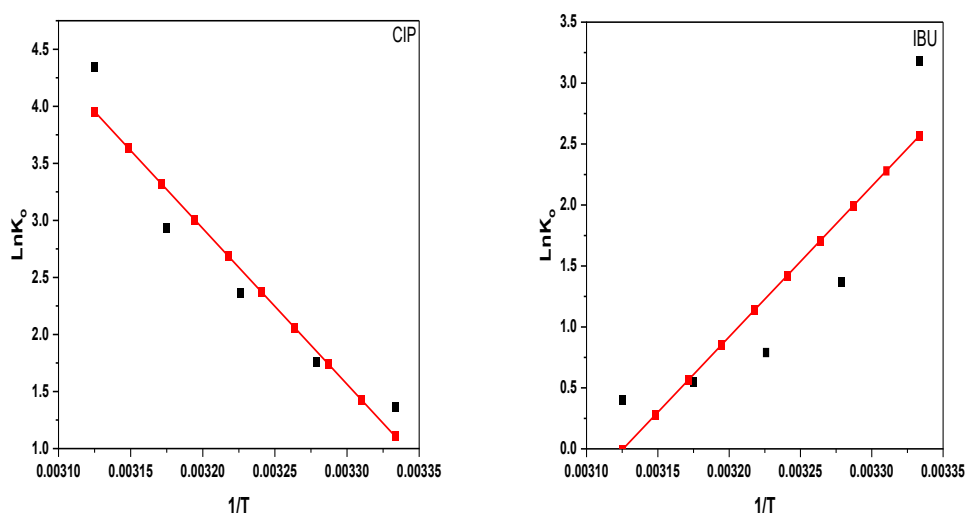


**Figure 14:** Van't Hoff plot for the adsorption of CIP and IBU

**Table 1:** Thermodynamic parameters for the adsorption of ciprofloxacin and ibuprofen

	C <sub>e</sub> (mg/L)	q <sub>e</sub> (mg/g)	K <sub>c</sub>	ΔG (J/mol)	ΔH (J/mol)	ΔS (J/mol)
CIP	1.134904	4.432548	3.90566	-2763.86		
	0.792291	4.603854	5.810811	-4702.92		
	0.449679	4.775161	10.61905	-6641.99	113580.101	387.8131812
	0.258244	4.870878	18.86153	-8581.06		
	0.06424	4.96788	77.33333	-10520.1		
IBU	0.203947	4.898026	24.01613	1913.11		
	1.125	4.4375	3.944444	3518.851		
	1.848684	4.075658	2.204626	5124.592	94431.3515	321.1482036
	2.243421	3.878289	1.728739	6730.333		
	2.506579	3.746711	1.494751	8336.074		

### Kinetics models

The kinetics of pharmaceutical adsorption were investigated using the pseudo first-order, pseudo-second order, interparticle diffusion, and Elovich kinetic models as presented on Figure 15. The parameters of the kinetic models as summarized on in Table 2 indicated that the Pseudo-First-Order Model exhibited a poor fit for ciprofloxacin ( $R^2 = 0.42245$ ) but a good fit for ibuprofen ( $R^2 = 0.99015$ ). In contrast, the Pseudo-Second-Order Model, based on chemisorption as the rate-limiting step, showed high  $R^2$  values for both drugs (ciprofloxacin: 0.99521, ibuprofen: 0.99015), indicating a good fit. The Interparticle Diffusion Model, which considers adsorbate transport to the surface, revealed relatively low  $R^2$  values for ciprofloxacin (0.55559) and ibuprofen (0.58528), suggesting other rate-controlling steps. The Elovich Model, describing chemisorption kinetics, showed moderate fits for both drugs (ciprofloxacin: 0.65612, ibuprofen: 0.66007), implying some chemisorption is occurring. Hence, the pseudo-second-order model provided the best fit, indicating chemisorption control of the adsorption process. The dominant mechanism was chemisorption, evidenced by strong interactions between pharmaceutical molecules and iron oxide nanoparticles (Ben Yahia, 2022). This interaction involves valence forces, as indicated by high  $R^2$  values (Dussan *et al.*, 2017; Bruschi *et al.*, 2020). The equilibrium adsorption capacities ( $q_e$  values) were high for both compounds, reflecting efficient adsorption. Additionally, higher rate constants ( $k_2$ ) suggest rapid removal of pharmaceuticals. The interparticle diffusion and Elovich models further support the efficiency of the adsorption process, providing insights into diffusion involvement and the degree of chemisorption (Edet & Ifelebuegu, 2020).

The adsorption of both ciprofloxacin and ibuprofen followed the pseudo-second-order kinetic model, indicating that chemisorption was the dominant mechanism. The interparticle diffusion model showed that surface interactions played a role, but were not the only rate-controlling step.

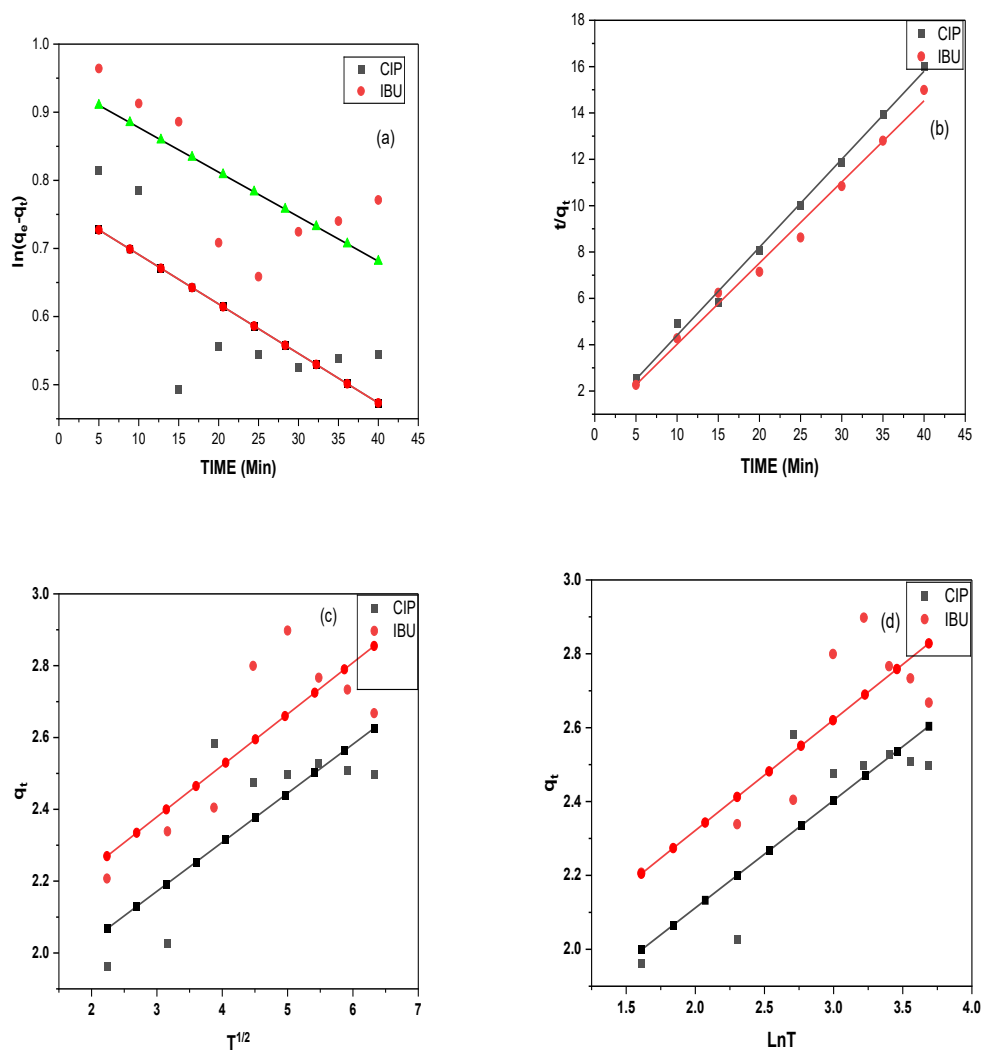


**Figure 15:** Kinetics for the adsorption of CIP and IBU (a) Pseudo first order (b) pseudo second order (c) interparticle diffusion (d) Elovich kinetic model.

**Table 2:** Kinetic models for the adsorption of Ciprofloxacin using the synthesized IONPs

Sn	Kinetic models	Parameters	Ciprofloxacin	Ibuprofen
1	Pseudo 1 <sup>st</sup> order	$q_e(\text{mg/g})$	2.14598	1.68502
		$k_1(\text{mg/g})(\text{l/mg})^{1/n}$	-0.00018	-0.00875
		$R^2$	0.42245	0.99015
2	Pseudo 2 <sup>nd</sup> order	$q_e(\text{mg/g})$	2.63317	2.85632
		$q_e^2$	6.93359	8.15860
		$k_2(\text{g/mgs})$	0.23696	0.23490
		$R^2$	0.99521	0.99015
3	Interparticle diffusion	$k_p(\text{mg/gmin}^{1/n})$	0.13656	0.14319
		$C(\text{mg/g})$	1.76198	1.94937
		$R^2$	0.55559	0.58588
4	Elovich	$a(\text{mg//gmin})$	55.7062	93.58215
		$B(\text{g/mg})$	3.4344	3.33533
		$R^2$	0.65612	0.66012

### Adsorption isotherms models

The adsorption isotherms for the removal of ciprofloxacin and ibuprofen were investigated using the Langmuir, Freundlich, and Temkin models as presented on Figures 16-18 and the parameters presented on Table 3. According to Ayawei *et al.* (2017), the Langmuir isotherm implies monolayer adsorption on a uniform surface with a finite number of identical sites. For ciprofloxacin, the Langmuir model revealed a high adsorption capacity ( $q_m$ ) of 4.87781 mg/g, a strong binding affinity with  $K_L$  of 0.91587 L/mg,  $R_L$  value of 0.01926 indicating highly favorable adsorption, and  $R^2$  of 0.92957 showing a good fit. Conversely, ibuprofen exhibited even higher adsorption capacity and affinity. In the case of the Freundlich isotherm, which describes adsorption on heterogeneous surfaces, ciprofloxacin showed favorable adsorption characteristics with a  $1/n$  value of 0.70444 and a  $K_F$  value of 2.30075, while ibuprofen displayed even higher values indicating a high adsorption capacity. The Temkin isotherm, which considers indirect adsorbate/adsorbent interactions, ciprofloxacin demonstrated heat of adsorption behavior different from ibuprofen, with respective  $RT/b$  and  $b$  values. The fit to the Temkin model was moderate for both compounds. Hence, the findings suggest that both ciprofloxacin and ibuprofen exhibit high adsorption capacities on iron oxide nanoparticles, with ibuprofen showing a greater capacity. The Langmuir and Freundlich models align well with ciprofloxacin's behavior, while the Freundlich model indicates a very high adsorption capacity for ibuprofen, likely due to its complex structure. The moderate fit of the Temkin model supports the influence of adsorbate-adsorbent interactions as observed in previous studies (Sharma & Dhiman, 2017; Pinto *et al.*, 2024).

Ciprofloxacin adsorption was best described by the Langmuir isotherm, suggesting monolayer adsorption on a homogeneous surface, while ibuprofen followed the Freundlich isotherm, indicating adsorption on a heterogeneous surface. These findings suggest different binding behaviors of the two pharmaceuticals on the nanoparticles.

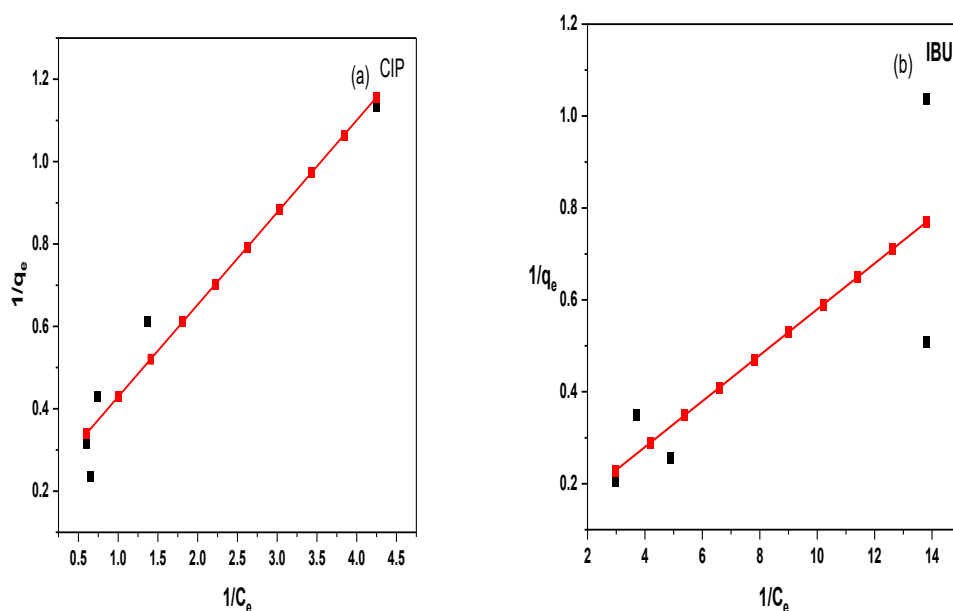


**Figure 16:** Langmuir adsorption isotherm of (a) CIP and (b) IBU

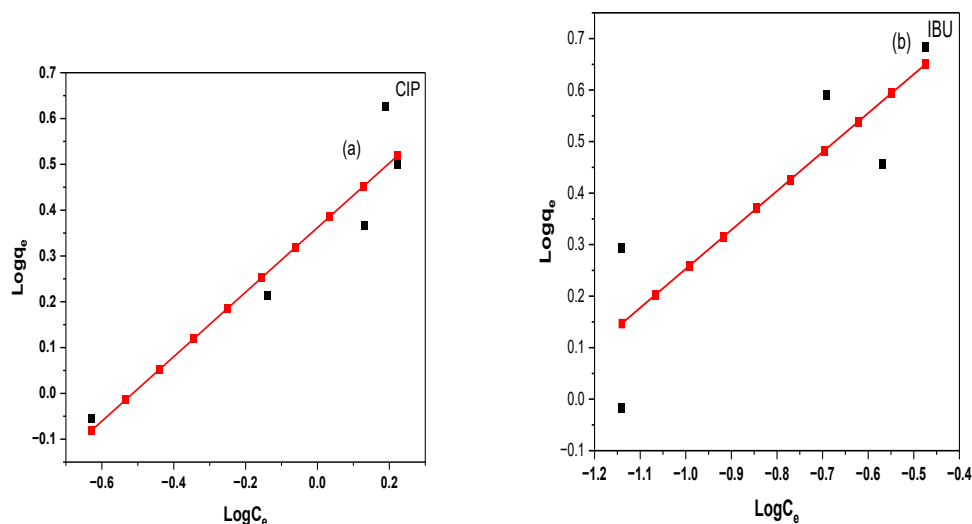


**Figure 17:** Freundlich adsorption isotherm of (a) CIP and (b) IBU

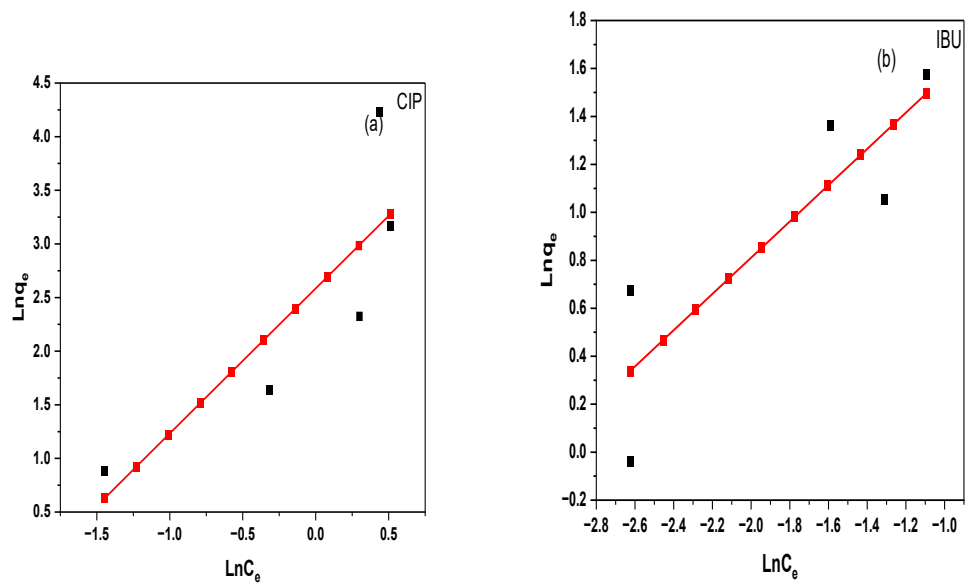


Figure 18: Temkin adsorption isotherm of (a) CIP and (b) IBU

Table 3: Adsorption isotherm parameters for the adsorption of ciprofloxacin and ibuprofen

Isotherm	Parameters	Ciprofloxacin	Ibuprofen
Langmuir	$q_m(\text{mg/g})$	4.87781	12.4906
	$K_L(\text{l/mg})$	0.91587	1.60312
	$R_L(\text{mg/l})$	0.01926	0.01901
	$R^2$	0.92957	0.55331
Freundlich	$1/n$	0.70444	0.75572
	$N$	1.41957	1.32324
	$K_f(\text{mg/g})(\text{l/mg})^{1/n}$	2.30075	10.2012
	$R^2$	0.8655	0.67365
Temkin	$RT/b$	1.35307	0.75572
	$\ln(a)$	2.58593	2.3225
	$a(\text{l/g})$	13.2756	10.2011
	$b(\text{J/mol})$	1832	3280.08
	$R^2$	0.62937	0.67635

Reusability of the adsorbent

This study evaluated the reusability of rice husk-derived iron oxide nanoparticles (RHNPs) as an adsorbent for the removal of ciprofloxacin and ibuprofen from water. The reusability was assessed through adsorption-desorption cycles over four successive applications. The



results showed a decline in adsorption efficiency from 69.65% to 66.65% for ciprofloxacin (a 4.30% decrease) and a 25.83% decline in ibuprofen adsorption efficiency by nanoparticles, reducing from 85.93% to 63.73%. This decline is likely due to the saturation of active adsorption sites and potential structural changes in the nanoparticles after repeated use (Zhu *et al.*, 2022). Despite this, the nanoparticles retain a moderate adsorption capacity, showcasing their resilience and feasibility for reuse in multiple cycles. Similar studies emphasize the practical advantages of reusability in water treatment technologies, despite efficiency losses (Ahmed *et al.*, 2021).

The ability to maintain 63.73% efficiency underscores the cost-effectiveness and environmental sustainability of reusing these adsorbents. Factors influencing efficiency loss, such as regeneration methods and potential competition with other contaminants, warrant further investigation to optimize reuse potential (Chen *et al.*, 2020). This balance between performance and sustainability demonstrates the practicality of the approach in real-world applications.

Compared to similar studies with chemically synthesized iron oxide nanoparticles, the repeatability of RHNP is relatively lower. This is mainly attributed to the variability in the composition of the rice husk extract, which can affect the consistency and stability of the synthesized nanoparticles (Nzereogu *et al.*, 2023). Additionally, the natural bioactive compounds in rice husk that act as reducing and stabilizing agents may undergo degradation or leaching during repeated adsorption-desorption cycles, impacting the adsorbent's performance (Alam *et al.*, 2020).

Despite this limitation, the study contributes potential advancements by promoting a green synthesis approach that utilizes an abundant agricultural byproduct, enhancing sustainability and cost-effectiveness. Furthermore, the observed adsorption efficiency and moderate decline in reusability suggest that RHNP can still be competitive, especially in applications where cost and environmental impact are critical considerations.

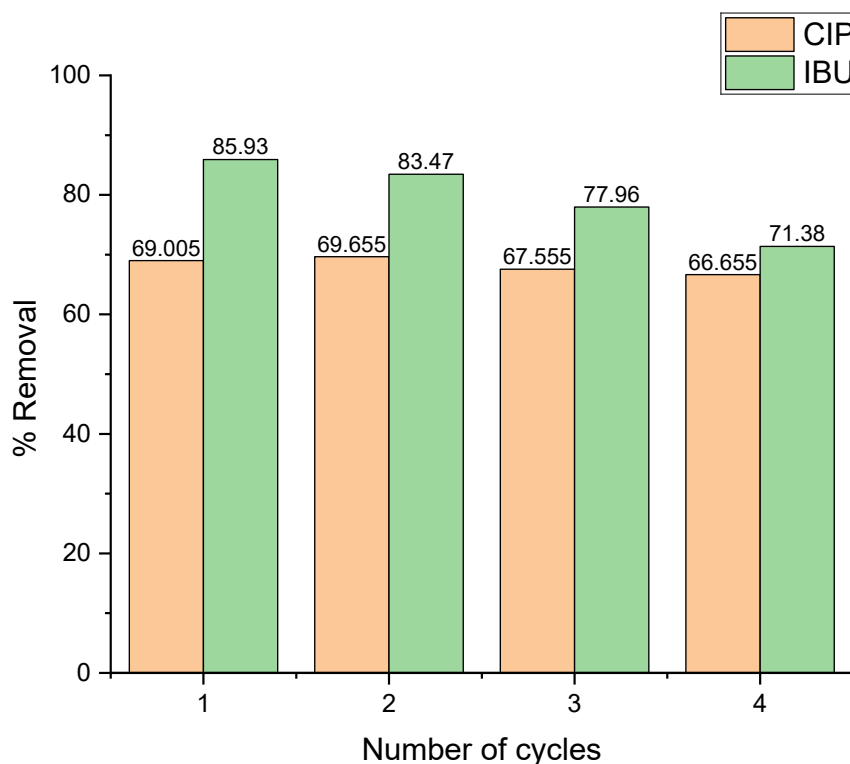


**Figure 19:** Recovery Reusability of the adsorbents

### Conclusion

In conclusion, the utilization of rice husk-derived iron oxide nanoparticles presents a promising approach for environmental remediation, particularly in the removal of pharmaceutical contaminants from water sources. The green synthesis method used produced nanoparticles with properties responsible for its high adsorption capacity, showcases their potential as sustainable adsorbents. The study's findings demonstrate the effectiveness of the nanoparticles in removing ciprofloxacin and ibuprofen, with considerations for factors such as pH, initial adsorbate concentration, contact time and temperature. Despite a slight decline in efficiency over successive cycles, the reusability of the nanoparticles underscores their practicality for long-term applications. The research highlights the significance of utilizing agrowaste materials for the synthesis of functional nanomaterials with promising implications for environmental remediation strategies. Future studies should optimize synthesis conditions by maintaining a reaction temperature of 60–80°C, a  $\text{FeCl}_3$ :  $\text{FeCl}_2$  ratio of 2:1 or 3:1, and an alkaline pH of 10–12 to enhance nanoparticle stability and adsorption efficiency. Extending reaction time, refining rice husk pre-treatment, and optimizing drying conditions can further improve performance and reusability for wastewater treatment.

**Conflict of Interest**

All the authors declared that there is no conflict of interest attached with this article.

**Ethical Approval**

Not applicable.

**Informed Consent**

Not applicable.

**Data availability**

The data used in this study is available on request.

**References**

- Adamu, H. I., Faruruwa, M. D., Adeyemi, M. M., Tomori, W. B., & Akorede, A. O. (2023). Plant Synthesized Iron Oxide Nanoparticles for Removal of Emerging Contaminant. *Chem Afri*, 1-14. <https://doi.org/10.1007/s42250-023-00822-0>
- Adegoke, K. A., Akinnawo, S. O., Adebuseyi, T. A., Ajala, O. A., Adegoke, R. O., Maxakato, N. W., & Bello, O. S. (2023). Modified biomass adsorbents for removal of organic pollutants: a review of batch and optimization studies. *Interna J of Environ Sci and Techno*, 1-30. <https://doi.org/10.1007/s13762-023-04872-2>
- Ahmadpour, A., Fallah, S., & Towfighi, J. (2019). Synthesis and characterization of nanostructured NiO/Al<sub>2</sub>O<sub>3</sub> catalyst for oxidative dehydrogenation of ethane. *J of the Iranian Chem Soc*, 16(2), 299-310. <https://doi.org/10.1007/s13738-018-1510-4>.
- Ahmed, M., Hassan, M., & Khan, R. (2021). Advances in nanoparticle reusability for pharmaceutical adsorption in water treatment. *Journal of Environmental Chemistry and Engineering*, 9(4), 1023-1034.
- Alam, M. M., Hossain, M. A., Hossain, M. D., Johir, M. A. H., Hossen, J., Rahman, M. S., ... & Ahmed, M. B. (2020). The potentiality of rice husk-derived activated carbon: From synthesis to application. *Processes*, 8(2), 203.
- Al-Musawi, T. J., Mahvi, A. H., Khatibi, A. D., & Balarak, D. (2021). Effective adsorption of ciprofloxacin antibiotic using powdered activated carbon magnetized by iron (III) oxide magnetic nanoparticles. *J of por mat*, 28, 835-852. <https://doi.org/10.1007/s10934-021-01039-7>
- Ayawei, N., Ebelegi, A. N., & Wankasi, D. (2017). Modelling and interpretation of adsorption isotherms. *J of chem*. <https://doi.org/10.1155/2017/3039817>
- Bachheti, R. K., Konwarh, R., Gupta, V., Husen, A., & Joshi, A. (2019). Green synthesis of iron oxide nanoparticles: cutting edge technology and multifaceted applications. *Nanomaterials and plant potentl*, 239-259. [https://doi.org/10.1007/978-3-030-05569-1\\_9](https://doi.org/10.1007/978-3-030-05569-1_9)
- Badawi, A. K., Abd Elkodous, M., & Ali, G. A. (2021). Recent advances in dye and metal ion removal using efficient adsorbents and novel nano-based materials: an overview. *RSC advances*, 11(58), 36528-36553.
- Bakatula, E. N., Richard, D., Neculita, C. M., & Zagury, G. J. (2018). Determination of point of zero charge of natural organic materials. *Environ Sci and Pol Research*, 25, 7823-7833. <https://doi.org/10.1007/s11356-017-1115-7>

- Balarak, D., Mahvi, A. H., Shim, M. J., & Lee, S. M. (2021). Adsorption of ciprofloxacin from aqueous solution onto synthesized NiO: isotherm, kinetic and thermodynamic studies. *Desalin Water Treat*, 212, 390-400. doi: 10.5004/dwt.2021.26603
- Baratta, M., Tursi, A., Curcio, M., Cirillo, G., Nezhdanov, A. V., Mashin, A. I., ... & De Filipo, G. (2022). Removal of Non-Steroidal Anti-Inflammatory Drugs from Drinking Water Sources by GO-SWCNT Buckypapers. *Molecules*, 27(22), 7674. <https://doi.org/10.3390/molecules27227674>
- Behzadi, S., Ghasemi, F., Ghalkhani, M., Ashkarran, A. A., Akbari, S. M., Pakpour, S., ... & Mahmoudi, M. (2015). Determination of nanoparticles using UV-Vis spectra. *Nanoscale*, 7(12), 5134-5139.
- Ben Yahia, M. (2022). An advanced physical modeling of adsorption mechanism of pharmaceutical compound on a biochar. *AIP Advances*, 12(3). DOI: [10.1063/5.0084620](https://doi.org/10.1063/5.0084620)
- Bruschi, M. L., & de Toledo, L. D. A. S. (2019). Pharmaceutical applications of iron-oxide magnetic nanoparticles. *Magnetochemistry*, 5(3), 50. <https://doi.org/10.3390/magnetochemistry5030050>
- Chen, W., Li, S., & Zhao, Y. (2020). Mechanisms of adsorption efficiency decline in nanoparticles: Implications for practical applications. *Water Science and Technology*, 82(5), 1060–1072.
- Dussán, K. J., Giese, E. C., Vieira, G. N., Lima, L. N., & Silva, D. D. (2017). Pharmaceutical and biomedical applications of magnetic iron-oxide nanoparticles. *Metal Nanoparticles in Pharma*, 77-99. DOI: [10.1007/978-3-319-63790-7\\_5](https://doi.org/10.1007/978-3-319-63790-7_5)
- Edet, U. A., & Ifelebuegu, A. O. (2020). Kinetics, isotherms, and thermodynamic modeling of the adsorption of phosphates from model wastewater using recycled brick waste. *Processes*, 8(6), 665. <https://doi.org/10.3390/pr8060665>
- Fahmy, H. M., Mohamed, F. M., Marzouq, M. H., Mustafa, A. B. E. D., Alsoudi, A. M., Ali, O. A., ... & Mahmoud, F. A. (2018). Review of green methods of iron nanoparticles synthesis and applications. *BioNanoScience*, 8, 491-503. <https://doi.org/10.1007/s12668-018-0516-5>
- Faisal, S., Jan, H., Shah, S. A., Shah, S., Khan, A., Akbar, M. T., Rizwan, M., Jan, F., Wajidullah, & Akhtar, N. (2021). Green synthesis of zinc oxide (ZnO) nanoparticles using aqueous fruit extracts of Myristica fragrans: their characterizations and biological and environmental applications. *ACS Omega*, 6(14), 9709–9722. <https://doi.org/10.1021/acsomega.1c00310>
- Farkas, N., & Kramar, J. A. (2021). Dynamic light scattering distributions by any means. *J of Nano Res*, 23(5), 120. <https://doi.org/10.1007/s11051-021-05220-6>
- Faruruwa, M. D., Adamu, H. I., Adeyemi, M. M., & Tomori, W. B. (2024). Green synthesis of iron (III) oxide (Fe<sub>3</sub>O<sub>4</sub>) Nanoparticles Using Citrus sinensis Peel Extract for the Removal of Ciprofloxacin in Water. *J of Appli Sci and Environ Manage*, 28(3), 823-839. DOI:[10.4314/jasem.v28i3.23](https://doi.org/10.4314/jasem.v28i3.23).
- Garau, G., Lauro, G. P., Diquattro, S., Garau, M., & Castaldi, P. (2019). Sb (V) adsorption and desorption onto ferrihydrite: influence of pH and competing organic and inorganic anions. *Environ Sci and Pollut Res*, 26, 27268-27280. <https://doi.org/10.1007/s11356-019-05919-z>
- Gomes, M. P. (2024). The Convergence of Antibiotic Contamination, Resistance, and Climate Dynamics in Freshwater Ecosystems. *Water*, 16(18), 2606. <https://doi.org/10.3390/w16182606>
- Ha, H. T., Phong, P. T., & Minh, T. D. (2021). Synthesis of iron oxide nanoparticle functionalized activated carbon and its applications in arsenic adsorption. *J of Analyt Methods in Chem*, 2021, 1-9. <https://doi.org/10.1155/2021/6668490>
- Hamdaoui, O., & Naffrechoux, E. (2007). Modeling of adsorption isotherms of phenol and chlorophenols onto granular activated carbon: Part I. Two-parameter models and equations allowing determination of thermodynamic parameters. *J of haz mat*, 147(1-2), 381-394. <https://doi.org/10.1016/j.jhazmat.2007.01.021>
- Javed, R., Zia, M., Naz, S., Aisida, S. O., Ain, N. U., & Ao, Q. (2020). Role of capping agents in the application of nanoparticles in biomedicine and environmental remediation: recent trends and future prospects. *J of Nanobiotech*, 18, 1-15. <https://doi.org/10.1186/s12951-020-00704-4>

- Kaasalainen, M., Aseyev, V., von Haartman, E., Karaman, D. Ş., Mäkilä, E., Tenhu, H., ... & Salonen, J. (2017). Size, stability, and porosity of mesoporous nanoparticles characterized with light scattering. *Nanoscale research letters*, 12, 1-10. <https://doi.org/10.1186/s11671-017-1853-y>
- Kumar Mohanta, P., Ripa, M. S., Regnet, F., & Jörisen, L. (2021). Effects of supports BET surface areas on membrane electrode assembly performance at high current loads. *Catalysts*, 11(2), 195. <https://doi.org/10.3390/catal11020195>
- Lunge, S., Singh, S., & Sinha, A. (2014). Magnetic iron oxide (Fe<sub>3</sub>O<sub>4</sub>) nanoparticles from tea waste for arsenic removal. *J of Magn and Magnetic Mat*, 19, 21–31. <https://doi.org/10.1016/j.jmmm.2013.12.008>.
- Mahdavi, M., Namvar, F., Ahmad, M. B., & Mohamad, R. (2013). Green biosynthesis and
- Mansouri, F., Chouchene, K., Roche, N., & Ksibi, M. (2021). Removal of pharmaceuticals from water by adsorption and advanced oxidation processes: state of the art and trends. *Appl. Sci.*, 11(14), 6659. <https://doi.org/10.3390/app11146659>.
- Mohamed Khalith, S. B., Ramalingam, R., Karuppannan, S. K., Dowlath, M. J. H., Kumar, R., Vijayalakshmi, S., Uma Maheshwari, R., & Arunachalam, K. D. (2022). Synthesis and characterization of polyphenols functionalized graphitic hematite nanocomposite adsorbent from an agro waste and its application for removal of Cs from aqueous solution. *Chemosphere*, 286(P1), 131493. <https://doi.org/10.1016/j.chemosphere.2021.131493>.
- Moradi, S. E., Haji Shabani, A. M., Dadfarnia, S., & Emami, S. (2016). Effective removal of ciprofloxacin from aqueous solutions using magnetic metal–organic framework sorbents: mechanisms, isotherms and kinetics. *J.I of the Iranian cheml soc*, 13, 1617-1627. <https://doi.org/10.1007/s13738-016-0878-y>
- National Center for Biotechnology Information (2023). PubChem Compound Summary for CID 2764,Ciprofloxacin.RetrievedOctober5,2023from <https://pubchem.ncbi.nlm.nih.gov/compound/Ciprofloxacin>
- Nguyen, D. T. C., Le, H. T. N., Do, T. S., Pham, V. T., Dai Tran, L., Ho, V. T. T., ... & Doan, V. T. (2019). Metal-organic framework MIL-53 (Fe) as an adsorbent for ibuprofen drug removal from aqueous solutions: response surface modeling and optimization. *J of Chem*. <https://doi.org/10.1155/2019/5602957>
- Nithya, K., Sathish, A., & Sivamani, S. (2023). In situ synthesis of mesostructured iron oxide nanoparticles embedded in L. camara: adsorption insights and modeling studies. *Biomass Conversion and Biorefinery*, 13(9), 7827-7838. <https://doi.org/10.1007/s13399-021-01764-8>
- Nsubuga, D., Kabenge, I., Zziwa, A., Yiga, V. A., Mpendo, Y., Harbert, M., ... & Wydra, K. D. (2023). Optimization of adsorbent dose and contact time for the production of jackfruit waste nutrient-enriched biochar. *Waste Disposal & Sustainable Energy*, 5(1), 63-74. <https://doi.org/10.1007/s42768-022-00123-1>
- Nzereogu, P. U., Omah, A. D., Ezema, F. I., Iwuoha, E. I., & Nwanya, A. C. (2023). Silica extraction from rice husk: Comprehensive review and applications. *Hybrid Advances*, 100111.
- Opotu, L. A., Inuwa, I. M., Wong, S., Ngadi, N., & Razmi, F. A. (2022). Errors and inconsistencies in scientific reporting of aqueous phase adsorption of contaminants: a bibliometric study. *Cleaner Materials*, 100100. <https://doi.org/10.1016/j.clema.2022.100100>
- Piccin, J. S., Dotto, G. L., & Pinto, L. A. A. (2011). Adsorption isotherms and thermochemical data of FD&C Red n 40 binding by chitosan. *Brazilian J of Chem Eng*, 28, 295-304. <https://doi.org/10.1590/S0104-66322011000200014>
- Pinto, F. R., Marcellos, C. F., Manske, C., & Barreto Jr, G. (2024). Statistical analysis of parameters and adsorption isotherm models. *Environmental Science and Pollution Research*, 1-14. DOI: [10.21203/rs.3.rs-3295601/v1](https://doi.org/10.21203/rs.3.rs-3295601/v1)

- Priya, Naveen, Kaur, K., & Sidhu, A. K. (2021). Green synthesis: An eco-friendly route for the synthesis of iron oxide nanoparticles. *Front in Nanotechno*, 3, 655062. <https://doi.org/10.3389/fnano.2021.655062>
- Rahman, M. M., Inaba, K., Batnyagt, G., Saikawa, M., Kato, Y., Awata, R., ... & Takeguchi, T. (2021). Synthesis of catalysts with fine platinum particles supported by high-surface-area activated carbons and optimization of their catalytic activities for polymer electrolyte fuel cells. *RSC advances*, 11(33), 20601-20611.
- Shakorfow, A. M., Al Mhanna, N., Atiya, M. A., Hassan, A. K., Kadhim, F. Q., Mahmoud, Z. A., & Abbas, A. H. (2023). Removal of Ciprofloxacin Antibiotic from Synthesized Aqueous Solution Using Three Different Metals Nanoparticles Synthesized Through the Green Method. *Al-Khwarizmi Engineer. Journ*, 19(3), 1-22. <https://doi.org/10.22153/kej.2023.02.002>
- Sharma, N., & Dhiman, N. (2017). Kinetic and thermodynamic studies for ciprofloxacin hydrochloride adsorption from aqueous solution on CuO nanoparticles. 10, 98-106.
- Singh, A., Pratap, S.G. & Raj, A.(2024) Occurrence and dissemination of antibiotics and antibiotic resistance in aquatic environment and its ecological implications: a review. *Environ Sci Pollut Res* 31, 47505–47529. <https://doi.org/10.1007/s11356-024-34355-x>
- Toncón-Leal, C. F., Villarroel-Rocha, J., Silva, M. T. P. D., Braga, T. P., & Sapag, K. (2021). Characterization of mesoporous region by the scanning of the hysteresis loop in adsorption-desorption isotherms. *Adsorption*, 27(7), 1109-1122. <https://doi.org/10.1007/s10450-021-00342-8>
- Vikram, S., Vasanthakumari, R., Tsuzuki, T., & Rangarajan, M. (2016). Investigations of suspension stability of iron oxide nanoparticles using time-resolved UV-visible spectroscopy. *J of Nano Res* 18, 1-24. <https://doi.org/10.1007/s11051-016-3570-3>
- Xing, X., Feng, J., Lv, G., Song, K., Mei, L., Liao, L., ... & Xu, B. (2015). Adsorption mechanism of ciprofloxacin from water by synthesized birnessite. *Advan in Mat Sci and Eng*, 2015. <https://doi.org/10.1155/2015/148423>
- Yadav, S., Nadar, T., Lakkakula, J., & Wagh, N. S. (2024). Biogenic Synthesis of Nanomaterials: Bioactive Compounds as Reducing, and Capping Agents. In *Biogenic Nanomaterials for Environmental Sustainability: Principles, Practices, and Opportunities* (pp. 147-188). Cham: Springer International Publishing. [https://doi.org/10.1007/978-3-031-45956-6\\_6](https://doi.org/10.1007/978-3-031-45956-6_6)
- Yeap, S. P., Lim, J., Ngang, H. P., Ooi, B. S., & Ahmad, A. L. (2018). Role of particle-particle interaction towards effective interpretation of Z-average and particle size distributions from dynamic light scattering (DLS) analysis. *J of nano and nanotechn*, 18(10), 6957-6964. <https://doi.org/10.1166/jnn.2018.15458>
- Zambri, N. D. S., Taib, N. I., Abdul Latif, F., & Mohamed, Z. (2019). Utilization of neem leaf extract on biosynthesis of iron oxide nanoparticles. *Molecules*, 24(20), 3803. <https://doi.org/10.3390/molecules24203803>
- Zhu, J., Wang, T., & Lin, M. (2022). Nanoparticle saturation and structural changes in repeated adsorption cycles: A critical review. *Environmental Nanotechnology, Monitoring, & Management*, 15, 89–98.